HardwareX 9 (2021) e00178

Contents lists available at ScienceDirect

HardwareX

journal homepage: www.elsevier.com/locate/ohx

Hardware Article

Low-cost stimulation resistant electromyography

Lachlan R. McKenzie *, Christopher G. Pretty, Benjamin C. Fortune, Logan T. Chatfield

Centre for Bioengineering, University of Canterbury, Christchurch, New Zealand

ARTICLE INFO

Article history:

Keywords:
EMG
Bio-sensing
Electrical stimulation
Rehabilitation
Blanking
AC coupler

ABSTRACT

Surface Electromyography (sEMG) is the non-invasive measurement of skeletal muscle contraction bio-potentials. Measuring sEMG of a stimulated muscle can prove particularly difficult due to large scale and long lasting stimulation-induced artefacts: if an sEMG device does not account for such artefacts, its measurements can be swamped and components damaged. sEMG has been used in a wide range of clinical and biomedical fields, providing measures such as muscular fatigue and subject intent. The recording of sEMG can prove difficult due to signal contamination such as movement artefact and mains interference.

There are very few commercial sEMG devices that contain protection against large stimulation voltages or measures to reduce artefact transient times. Furthermore, most commercial or research level designs are not open source; these designs are effectively an inflexible black box to researchers and developers.

This research presents the design, test and validation of an open source sEMG design, able to record muscle bio-potentials concurrently to electrical stimulation. The open source, low-cost nature of the design provides accessibility to researchers without the time and cost associated with design development. The design has been tested on the forearms of four able-bodied subjects during 25 Hz constant current stimulation, and has been shown to record subject volitional sEMG and M-wave without saturation.

Specifications table:

Hardware name	*SARSE (Stimulation Artefact Reducing Surface Electromyography) Sensor*
Subject area	• *Bio-engineering* • *Mechatronics Engineering* • *Electrical Engineering* • *Bio-mechanics*
Hardware type	• *Electromyography* • *Bio-sensing* • *Bio-instrumentation* • *Field measurements and sensors*
Open source license	*Creative Commons Attribution-NONCommercial-ShareAlike 4.0 International*
Cost of hardware	*USD $145 (for one), USD $548 (for five)*
Source file repository	https://doi.org/10.17605/OSF.IO/P5DSW

* Corresponding author.
E-mail address: lachlan.mckenzie@pg.canterbury.ac.nz (L.R. McKenzie).

https://doi.org/10.1016/j.ohx.2021.e00178
2468-0672/

1. Hardware in context

Bioelectrical signals are widely used throughout commercial technology as well as in research. One such signal is surface electromyography (sEMG), a non-invasive technique applied to study skeletal muscle contraction, detecting the electrical activity in contracting muscle cells [1]. The electrical activity captured by sEMG is a bipolar signal with amplitude $\leqslant$ 10 mV pk-pk and usable energy within 0–500 Hz, but predominantly within the 50–150 Hz range [2]. sEMG has been used to provide measures such as muscular torque, muscular fatigue, and subject intent [3–5]. For these properties, sEMG is utilised in many fields, including bio-mechanics, sport-science, and rehabilitation.

Due to the low amplitude of the bio-potential signal, sEMG can be contaminated by several forms of interference, such as mains supply interference and movement artefact. In stroke rehabilitation use, sEMG is often used alongside functional electrical stimulation (FES). However, due to the nature of FES, the sEMG signal becomes contaminated with interference. Such interference is elicited by two predominant artefact sources: stimulation artefacts and M-wave artefact [6,7]. If an sEMG device does not account for such artefacts, meaningful data will be lost and the device components can be damaged. Therefore, there is increasing focus on stimulation resistant sEMG devices and artefact reduction techniques.

The sEMG device outlined in this paper consists of an input protection stage, artefact detection channel, and sEMG recording channel. The sEMG recording channel is based on the design by Fortune et al. [8], modified to include input protection, artefact suppressing hardware, and to accommodate $\pm$15 V rails on its pre-amplification stage. The system utilises pre-gelled, conductive carbon-film surface electrodes. A high-level system overview is depicted in Fig. 1.

2. Hardware description

Most commercial, research-level sEMG devices are not open source hardware and are costly. Additionally, their amplification and filtering stages are not divulged: in this manner, most commercial sEMG devices are effectively black boxes. For users, this means that these devices are generally inflexible and may not be suitable for their intended application. To the authors knowledge, very few sEMG devices are compatible with electrical stimulation, or can concurrently record sEMG from a stimulated muscle.

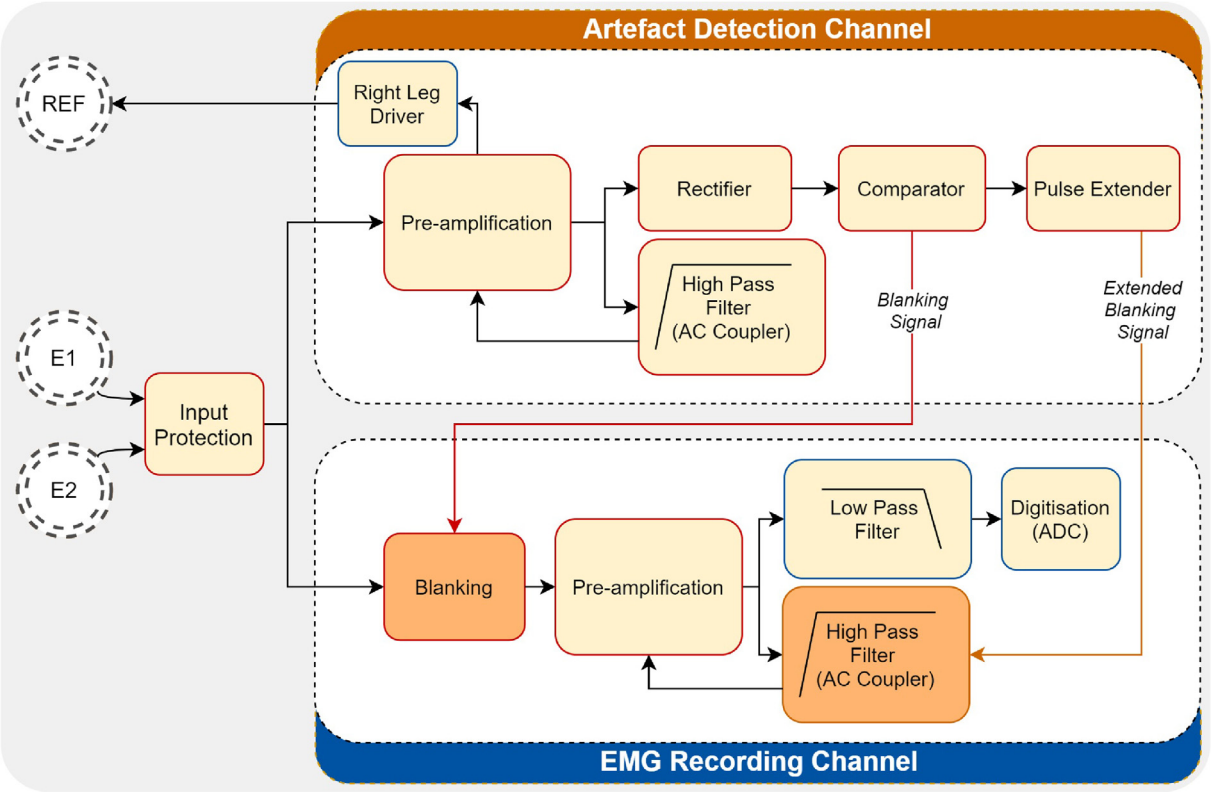

Fig. 1. System overview block diagram. Blocks with dark orange fill contain artefact suppressing features. Blocks with a blue outline represent sections designed by Fortune et al. [8]. E1, E2, and REF are the electrodes placed on the user for measurement. (For interpretation of the references to colour in this figure legend, the reader is referred to the web version of this article.)

There is a need for low-cost, flexible, and open-hardware sEMG designs, that can record from a stimulated muscle: the presented sEMG device has been designed to reflect these requirements. The design possesses an sEMG pre-amplifier topology with hardware to detect and to minimise stimulation artefact transients.

Artefact detection and suppression hardware is followed by an adjustable gain band-pass filter, 24-bit sigma delta analog to digital converter (ADC), and right leg driver (RLD). The adjustable-gain band-pass filer provides flexibility towards varying application environments, whilst the RLD attenuates EMI in real-time and the ADC outputs high-accuracy digitised sEMG. For more information on the sEMG signal-processing chain, see Fortune et al. [8].

- *Stimulation Resistance and Artefact Suppression*
  For applications such as monitoring (e.g. muscular torque, muscular fatigue) and control (e.g. neuro-prosthetic control), the volitional or stimulation elicited sEMG signal is often used. In order to facilitate these applications in a space-efficient manner, there is a requirement for same-muscle sEMG recording and stimulation. The main obstacle to recording from stimulated muscle are large-scale artefacts due to the stimulation that corrupt the sEMG signal; therefore, artefact reduction techniques have become increasingly paramount.
  The the authors knowledge, there are very few commercial devices that contain protection against large stimulation voltages or measures to reduce artefact transient times. In the presence of electrical stimulation, typical sEMG designs will therefore be damaged and volitional sEMG recordings saturated. Techniques for amplifier protection and artefact suppression have been explored in literature; however, these designs often rely on fixed timings for artefact suppression [9,10] or utilise low-gains to avoid amplifier saturation [11,12]. Furthermore, the designs are typically not open-source, with little more than high-level system overviews provided [13–15].
  The sEMG device presented in this work utilises a resistor-diode network to protect its pre-amplifier inputs from high stimulation voltages. Switching networks are used to blank the pre-amplifier inputs and to alter its feedback network upon the detection of stimulation artefact. These features protect the sEMG amplifiers from saturation and prevent long transients due to the system's filter responses. See Section 5.2.4 for more detail on these system components.
- *Flexibility*
  The gain of the sEMG device should be adjustable to allow for variable bio-potential amplitude arising from factors such as electrode spacing, strength of contraction, muscle of interest, and the electrode-skin interface. The design outlined in this paper contains an adjustable gain stage that does not affect the filtering characteristics of the device [8].
  Magnitude of the stimulation artefacts are also dependant on factors such as electrode spacing and the electrode-skin interface, as well as the stimulator and sEMG amplifier designs. The artefact detection channel should be able to accommodate this variability. A flexible artefact detection threshold is utilised in this work, adjustable via potentiometer, detailed in Section 5.2.3.
- *Cost*
  The high cost of commercial sEMG technology, some costing up to 20,000€, can be prohibitive [16]. While low-cost sEMG is becoming more readily available, the designs are limited by inadequate filtering techniques and vulnerability to stimulation.

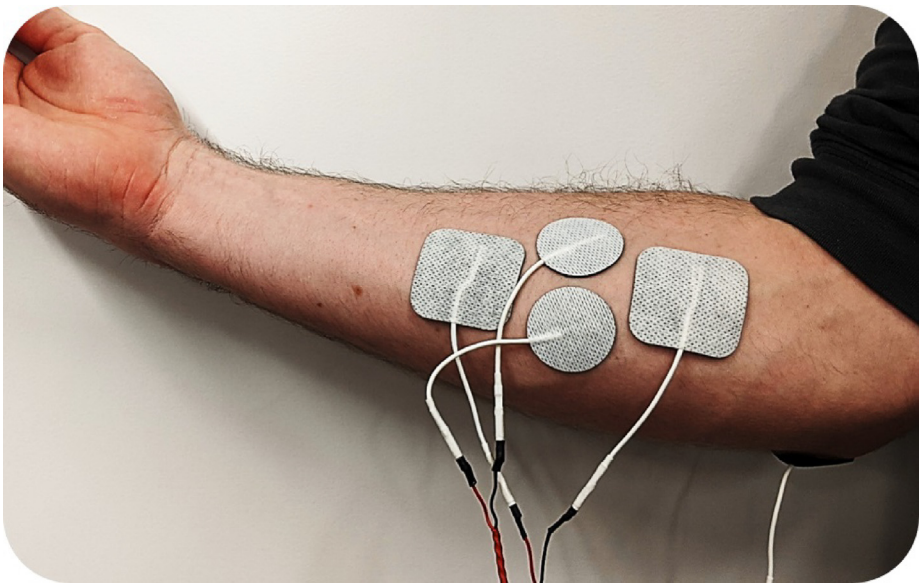

Fig. 2. Electrode configuration: Square stimulation electrodes (40 mm × 40 mm) are placed on the forearm longitudinally, with round sEMG electrodes (30 mm × 30 mm) placed in-between. The RLD electrode is placed on the elbow.

This design is low-cost, USD $145 for one, USD $548 for five. The design is open-source. Design choices behind stimulation artefact detection and suppression are provided in this documentation, and design choices for the sEMG signal chain are presented in Fortune et al. [8]. In this manner, the presented documentation allows future researchers and developers to more effectively utilise the design towards their intended application, saving time and money.

3. Design files

3.1. Design files summary

Design filename	File type	Open source license	Location of the file
sEMGArtefactSup.pdf	*PDF Schematic*	*CC BY-NC-SA 4.0*	https://doi.org/10.17605/OSF.IO/P5DSW
sEMG_BOM.csv	*BOM Spreadsheet CSV*	*CC BY-NC-SA 4.0*	https://doi.org/10.17605/OSF.IO/P5DSW
sEMG_Gerber.zip	*Gerber and Drill*	*CC BY-NC-SA 4.0*	https://doi.org/10.17605/OSF.IO/P5DSW
sEMG_Example_ Code.ino	*Arduino Script*	*CC BY-NC-SA 4.0*	https://doi.org/10.17605/OSF.IO/P5DSW

3.2. Schematic files

The sEMG circuit was developed using KiCad (version 5.0.2). Kicad is an open source software suite for Electronic Design Automation (EDA), licensed under GNU GPL v3. A PDF plot of the project schematics is included (sEMGArtefactSup.pdf).

3.3. Gerber and drill files

Gerber and drill files for the PCB are provided in sEMG_Gerber.zip. The files are compiled with JLCPCB as the intended manufacturer.

3.4. Bill of materials

A complete bill of materials (BOM) for the PCB is included, in spreadsheet form.

3.5. Arduino file

An Arduino file is provided that contains example code to configure the ADC and capture ADC data, as detailed in [8].

4. Bill of materials

A complete bill of materials has been included as an editable spreadsheet file.

5. Build instructions

5.1. Overview

An overview of the build process for the sEMG PCB is outlined below.

1. Order components and PCB. Components along with their supplier and part-number can be found in sEMG_BOM.csv. The PCB and stencil can be ordered using the gerber files provided in sEMG_Gerber.zip through JLCPCB (www.JLCPCB.com) or alternative PCB manufacturer.
2. Populate the PCB with components. Note: this process is easiest using the stencil and a re-flow oven for the surface mount components, and hand soldering for through-hole components.
3. Attach sEMG measurement electrodes to the PCB header labelled “Anode” and “Cathode”. Attach the reference electrode to the PCB header labelled “RLD”. Measurement and RLD electrode header positions are depicted in Fig. 3 as A and B, respectively.
4. Load the sEMG_Example_Code.ino program onto the micro-controller to obtain ADC data.

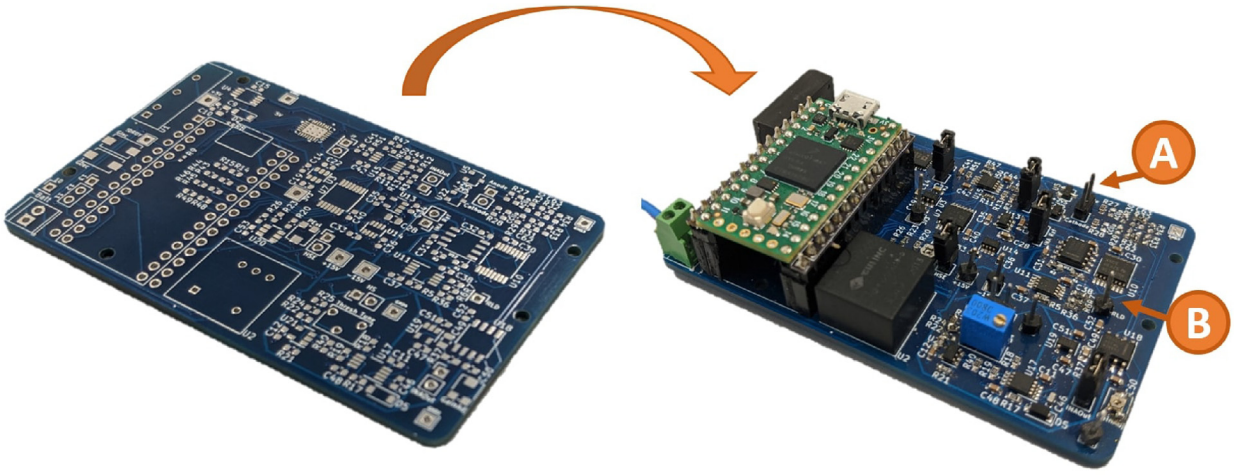

Fig. 3. Assembly of the sEMG device. Measurement and RLD electrode headers are located at A and B, respectively.

5.2. Design decisions

5.2.1. Power supply

The device presented in this work, unlike that described by Fortune et al. [8], is not designed to have active electrodes i.e. the recording device is not built into the electrodes: the PCB board size is therefore less restricted. Given the extra PCB board space, the design can include isolated power supplies and accommodate larger voltage rails.

The device is designed to operate from a single 12 V supply. The input regulators for the design differ from those in [8]: an isolated 5 V supply (U9:PDM1-S12-S5-S) and an isolated $\pm 15V$ supply (U10:PQP3-D12-D15-D) are used. The isolated nature of the on-board regulators allow the device to be safely powered by battery or an AC-powered bench-top supply.

The $\pm 15V$ rails are utilised for a number of reasons. Higher rail voltages allow for a larger pre-amplifier gain, taking advantage of the instrumentation amplifier's common-mode rejection ratio (CMRR) without causing saturation. Higher rails are also useful as the AC-coupler can account for larger electrode DC offsets: this is often an issue when stimulation is present on the recorded muscle. The low-pass filter and ADC stages are powered by the +2.5 V regulator (U12, REG710) and −2.5 V regulator (U11, LTC1550) as in [8].

5.2.2. System components adapted from Fortune et al.

A number of system components have been adopted from Fortune et al. [8], with minor alterations. These components are represented by the blocks with a blue outline in Fig. 1: the Right Leg Driver (RLD), low-pass filter, and digitisation (ADC). The minor alteration are as follows:

- RLD supply rails: The RLD rails are powered through a ± 15 V supply. This alteration follows as the recording pre-amplifier and AC-coupler are also powered off the ± 15 V supply.
- Op-amp selection: Two dual op-amp package OPA1602 (U1, U4) are used instead of the quad op-amp LT6204 for RLD and filtering sections. This substitution was made to allow cleaner routing of the PCB. The OPA1602 allows for ± 2.25 V to ± 18 V supplies, is rail-to-rail input and output, unity gain stable, and has a gain bandwidth product of 35 MHz.
- Low-pass filter adjustable gain: Adjustable gain of the low-pass anti-aliasing filter is still achieved through the AD5222 digital potentiometer (U17): However, control of the digital potentiometer is achieved through the micro-controller GPIO pins, rather than the ADC GPIO pins. This alteration is made for ease of PCB routing.

5.2.3. Artefact detection channel

The artefact detection channel is responsible for producing artefact suppression signals for the design. The signal timings are characterised through threshold detection of the artefact contaminated signal.

Pre-amplifier (U2: INA828)

An instrumentation amplifier is used to amplify the differential electrode voltage with respect to a reference. This is performed by the INA828, as depicted in Fig. 4. Note, the INA828 is the second generation of the INA128 instrumentation amplifier used in Fortune et al. [8].

The INA828 was chosen for its high common-mode rejection ratio (minimum of 130 dB over the pass-band) and low noise (7 nV/Hz). The output of the INA828 is AC coupled to remove any DC offset within ± 15 V rails. The amplifier gain is set by an external resistor by equation $G = 1 + \frac{50k\Omega}{R_G}$. The gain of the instrumentation amplifier is set to $\sim$369 V/V via gain resistance of

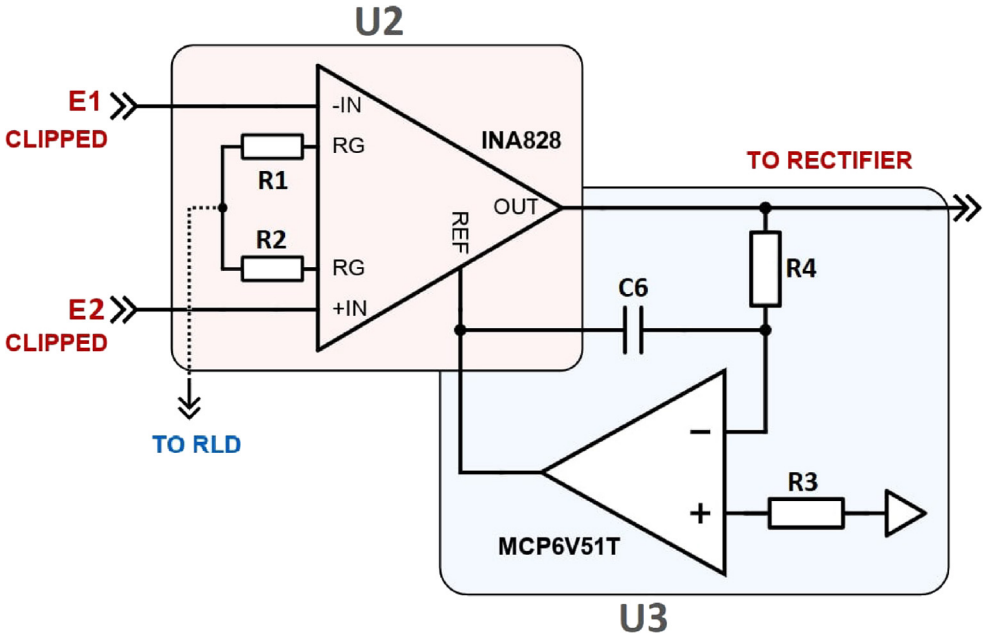

Fig. 4. Basic pre-amplifier topology. The red section indicates the instrumentation amplifier and gain resistor. The blue section indicates the AC-coupler. (For interpretation of the references to colour in this figure legend, the reader is referred to the web version of this article.)

136Ω. The gain resistance is formed by two 68Ω resistors (R1, R2), allowing the common-mode voltage to be accessed by the right leg driver (RLD).

AC Coupler (U3: MCP6V51T-E/OT)

The AC coupler is an integrating op-amp circuit that provides closed-loop feedback to the instrumentation amplifier's reference pin, Fig. 4. The AC coupler acts to remove DC offset and attenuate low-frequency noise from the instrumentation amplifier's output. The frequency response of the AC coupler is the same as a first-order low-pass RC filter, $F_C = \frac{1}{2\pi RC}$. A ~325 Hz frequency cut-off is obtained by using a 47 nF (C6) capacitor and 10 kΩ resistor (R4). The frequency cut-off is set above the main sEMG spectra to avoid triggering of artefact detection thresholds by volitional contractions. A compensation resistor (R3) equal to the integrator resistor is applied.

Rectifier

As the EMG signal is bipolar in nature, the output of the instrumentation amplifier needs to be rectified before the Schmitt trigger stage. A precision full-wave rectifier topology is utilised, as outlined in [17]. This design topology is used for its ability to output with minimal distortion near transition regions.

Schmitt trigger (U6: TLV1701)

The rectified EMG signal is passed to a Schmitt trigger to generate the blanking signal for the EMG recording channel. The Schmitt trigger's reference is set by an external voltage divider. Stimulation artefact is prone to vary with changes such as electrode configuration and electrode-skin interface. As such, it is desirable to have an adjustable threshold for artefact detection. The reference is manually adjustable via a 20 turn trimmer potentiometer RV1, see Fig. 5a.

The response of the Schmitt trigger is illustrated in Fig. 5b. The blanking signal is pulled low when stimulus is detected (when the rectifier output exceeds the high trigger threshold). The blanking signal will return high once the rectifier output falls below the lower threshold. The red shaded section in Fig. 5b represents the hysteresis region of the Schmitt trigger, which is useful for avoiding output jitter. The Schmitt trigger output passes through a voltage divider (R19, R20) to shift the output level to the +3.3 V pulse extender and switching logic levels. The Schmitt trigger output signal is fed as a blanking signal for the EMG recording channel, see Section 5.2.4.

Pulse Extender (U5: LTC6994)

A programmable delay block is used to delay the rising edge of the Schmitt trigger signal by ~0.5-8 ms, Fig. 6. The extended signal is used to alter the recording channel's AC-coupler time constant during stimulation. The extension time is set manually via trimmer potentiometer. More information is provided in Section 5.2.4.

5.2.4. EMG recording channel

The EMG recording channel is responsible for recording the user's volitional EMG. The channel contains elements for stimulation artefact suppression that are controlled by blanking signals, Section 5.2.3.

Pre-amplifier (U15: INA828)

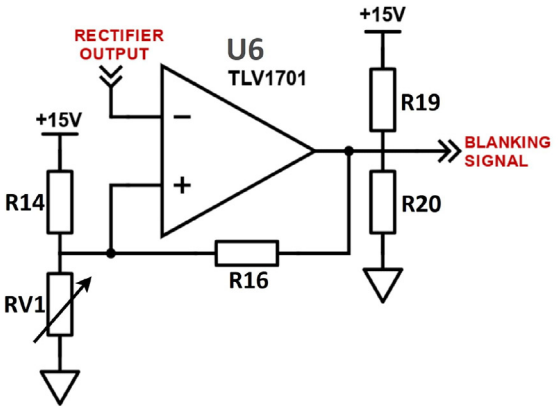

(a) Schmitt trigger topology

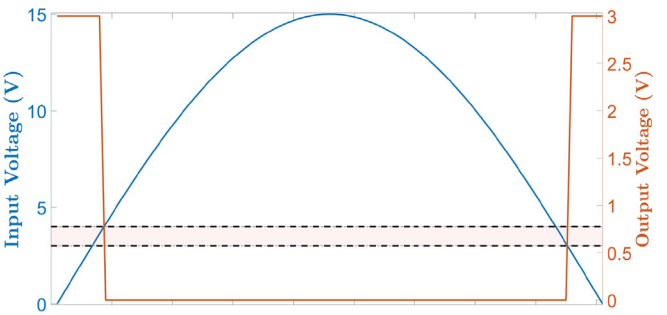

(b) Example: Blue represents the input voltage, and orange represents the Schmitt trigger output. The black dashed lines represent the high and low triggering voltages

Fig. 5. Schmitt trigger topology and output waveform.

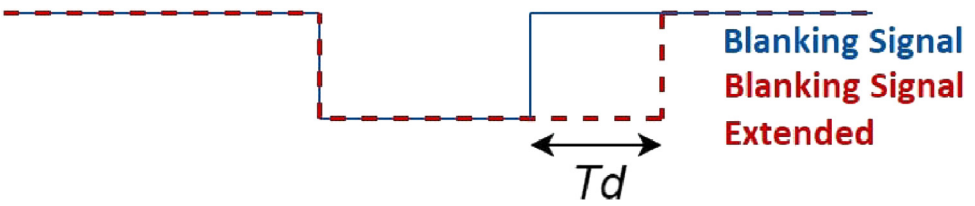

Fig. 6. Delay block output: Blue line represents Schmitt trigger output. Red dashed line represents the delay block output. Td is the delay time, adjustable from 512 μs to 8 ms. (For interpretation of the references to colour in this figure legend, the reader is referred to the web version of this article.)

The EMG recording pre-amplifier is similar to the artefact detection pre-amplifier, with modifications for stimulation artefact suppression. An overview of the pre-amplifier is depicted in Fig. 7. Alterations to the detection pre-amplifier topology are highlighted by the orange-filled sections, U14 and U16.

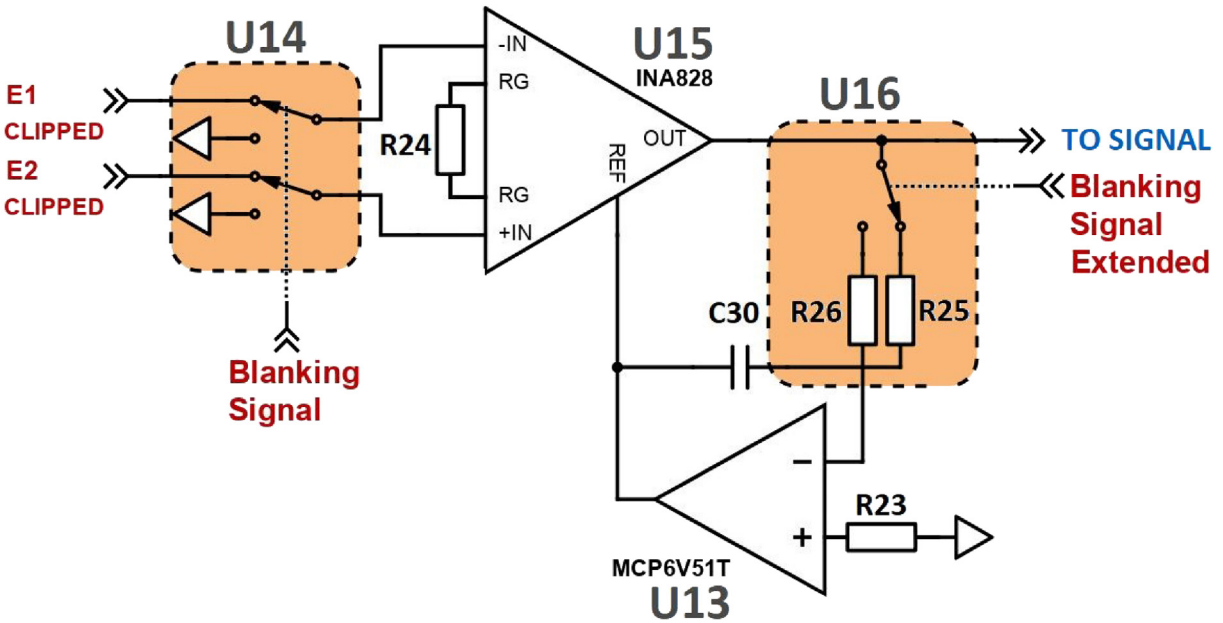

Fig. 7. EMG recording preamplifier chain.

The gain is nominally set to ~418 through an external 120Ω resistor (R24). DC electrode offset-voltages of up to ~36 mV can be tolerated at this gain, before a DC offset is generated at the pre-amplifier output.

Artefact suppression hardware

Single-pole dual-throw switches, U14 and U16, are placed in the EMG recording pre-amplifier chain to suppress stimulation artefact, see Fig. 7. The switches are controlled via the blanking signals generated by the artefact detection chain, Section 5.2.3.

- *Amplifier Input Blanking Switches (U14: TMUX6136)*
  The pre-amplifier can be easily saturated by stimulation artefacts, thus lengthening the recovery time in which volitional EMG cannot be measured [18,19]. Switches U14, depicted in Fig. 7, are used to shunt the pre-amplifier inputs to ground during stimulation. The switches protect the pre-amplifier from the stimulation artefact pulses, and therefore allow higher pre-amplifier gains without output saturation. The TMUX6136 dual analog switch is chosen due to it's low leakage current (0.5pA), fast transition times (66 ns), and low charge injection (-0.4pC).
  The switch timing is determined by the detection-Schmitt trigger stage which outputs a blanking signal whenever the electrode differential voltage exceeds a set threshold, Section 5.2.3.
- *Integrator Time Constant Switch (U16: TMUX6119)*
  The isolated use of pre-amplifier input blanking can cause further artefacts to enter the system: a discharge curve is generated as the system exits the blanking phase, due to a sharp change in signal level, seen as a step by the system's filtering amplifiers [20,13,21].
  In particular, the AC-coupler is of interest as it defines the high-pass characteristics of the pre-amplifier. When recording with no stimulation present,the AC coupler is configured to have a 20 Hz corner frequency. In this configuration, the AC coupler will remove DC offset and movement artefacts; however, the low corner frequency will introduce a slow exponential tail in response to a step input or impulse.
  Switch U16, depicted in Fig. 7, is used to switch the AC coupler time-constant, giving it an approximate ~10 kHz low-pass corner frequency. Essentially, the AC-coupler will track the output of the pre-amplifier and feed it back into the reference pin, giving the pre-amplifier fast recovery from step input or impulse. The TMUX6119 analog switch is chosen, again for low leakage currents (0.5pA), low charge injection (0.19pC), and fast transition times (68 ns).
  An extended blanking signal (see Section 5.2.3) is used to control switch U16. As the extended signal is used, the AC-coupler can absorb the voltage step and transients as pre-amplifier blanking finishes.

6. Operation instructions

6.1. Tuning stimulation artefact detection

Tuning of the artefact detection threshold is set through a 20 turn variable resistor (RV2) labelled as "Thresh Tune" on the PCB. The potentiometer should be trimmed to a level in which stimulation artefact is blanked, but voluntary contractions do not trigger the blanking.

Triggering is seen as a falling edge on the hold signal, see Fig. 5b. The hold signal is most easily measured using an oscilloscope probe on the "HS" header. If an oscilloscope is not available, the hold signal can be monitored on the microcontroller's digital pin 24.

6.2. Software

An example script "sEMG_Example_Code.ino" has been developed to obtain ADC data and to separate volitional sEMG from residual artefacts, using a Teensy4.0. The code is commented to outline why each instruction is performed.

6.2.1. Existing code for data acquisition

The code to extract ADC data is provided by Fortune et al. [8]: As the same ADC is utilised, the code for configuring ADC registers is the same.

7. Validation and characterisation

Electrodes for sEMG and stimulation were placed on the forearm of four able-bodied male subjects, aged 25–26. The electrode configuration, Fig. 2, has the sEMG electrodes perpendicular to the muscle fibre direction, between the stimulation electrodes. As the sEMG electrodes are perpendicular to the muscle fibre direction, there is slight reduction in sEMG signal strength [22]. However, the stimulation artefact and m-wave posses much higher common mode components and can be more easily rejected by the pre-amplifiers [23–25]. Additionally, the perpendicular orientation of the sEMG electrodes creates a more compact configuration than if they were placed along the muscle fibre direction. This is especially useful when applied to small muscle groups such as the forearm.

Sub-maximal isotonic contractions were recorded from the subjects concurrently to constant-current stimulation. Biphasic stimulation was delivered at a 25 Hz frequency and pulse-width of 200 μs per phase. The stimulation amplitude was delivered at a level that induced tetanic contraction and was comfortable for each subject. These amplitudes were determined prior to the trial and ranged between 7.5 mA and 9.5 mA.

The raw sEMG data recorded from the device is depicted in Fig. 8. From this data, it can be seen that the device captures each subject's sEMG signal without saturating. The left column of Fig. 8 shows the device output signal for each subject over three isotonic contractions. The right column shows a segment of the left column's data, corresponding to three stimulation

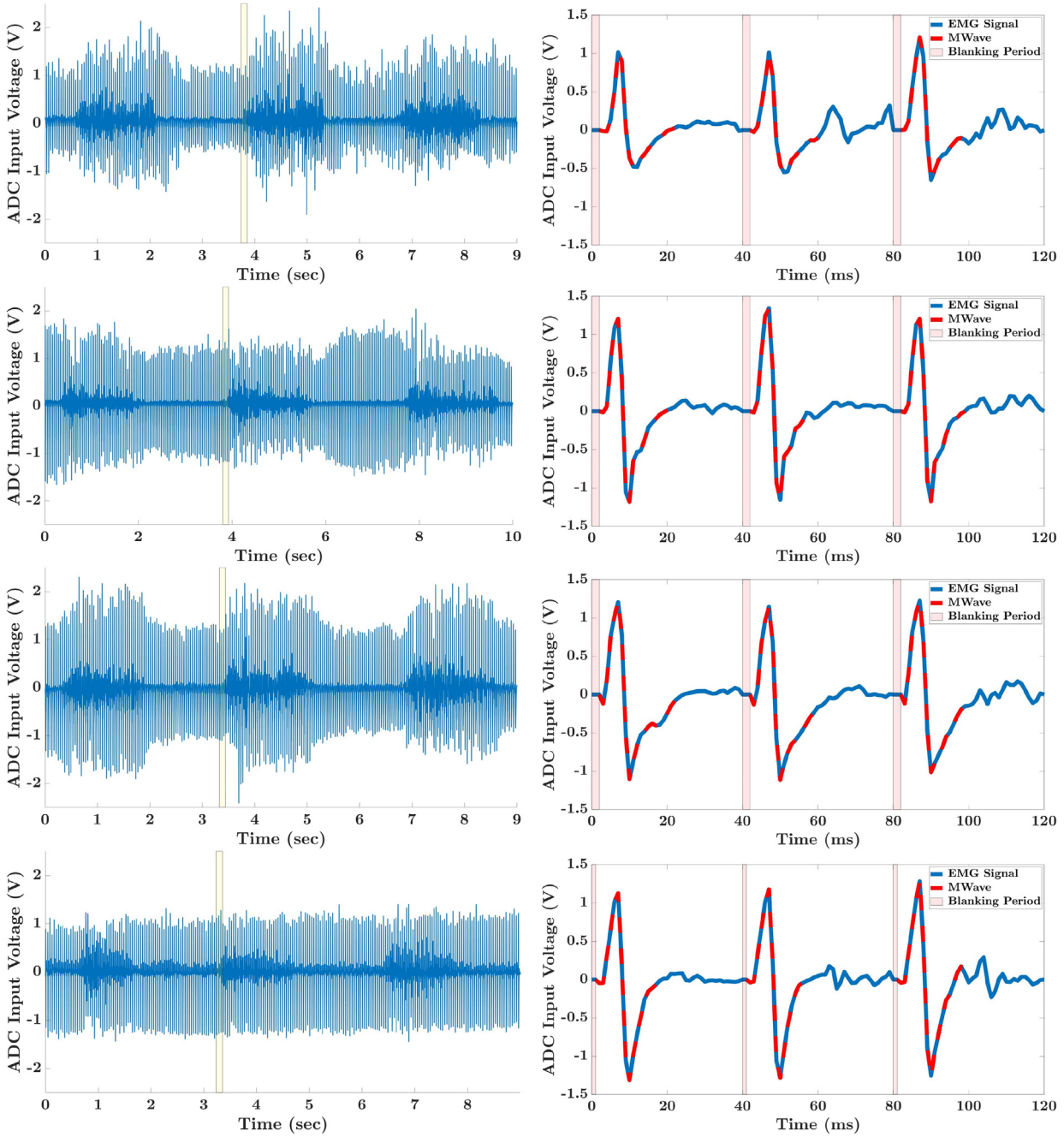

Fig. 8. Raw sEMG data recorded from four subjects. Left column: sEMG captured over three isotonic contractions. Right: Segments of the subject's data at the start of isotonic contraction, highlighted in yellow, spanning three stimulation periods. This data shows the blanking of the stimulation artefact, the superposition of M-Wave and volitional sEMG, and the volitional sEMG's increase in energy as isotonic contraction begins. (For interpretation of the references to colour in this figure legend, the reader is referred to the web version of this article.)

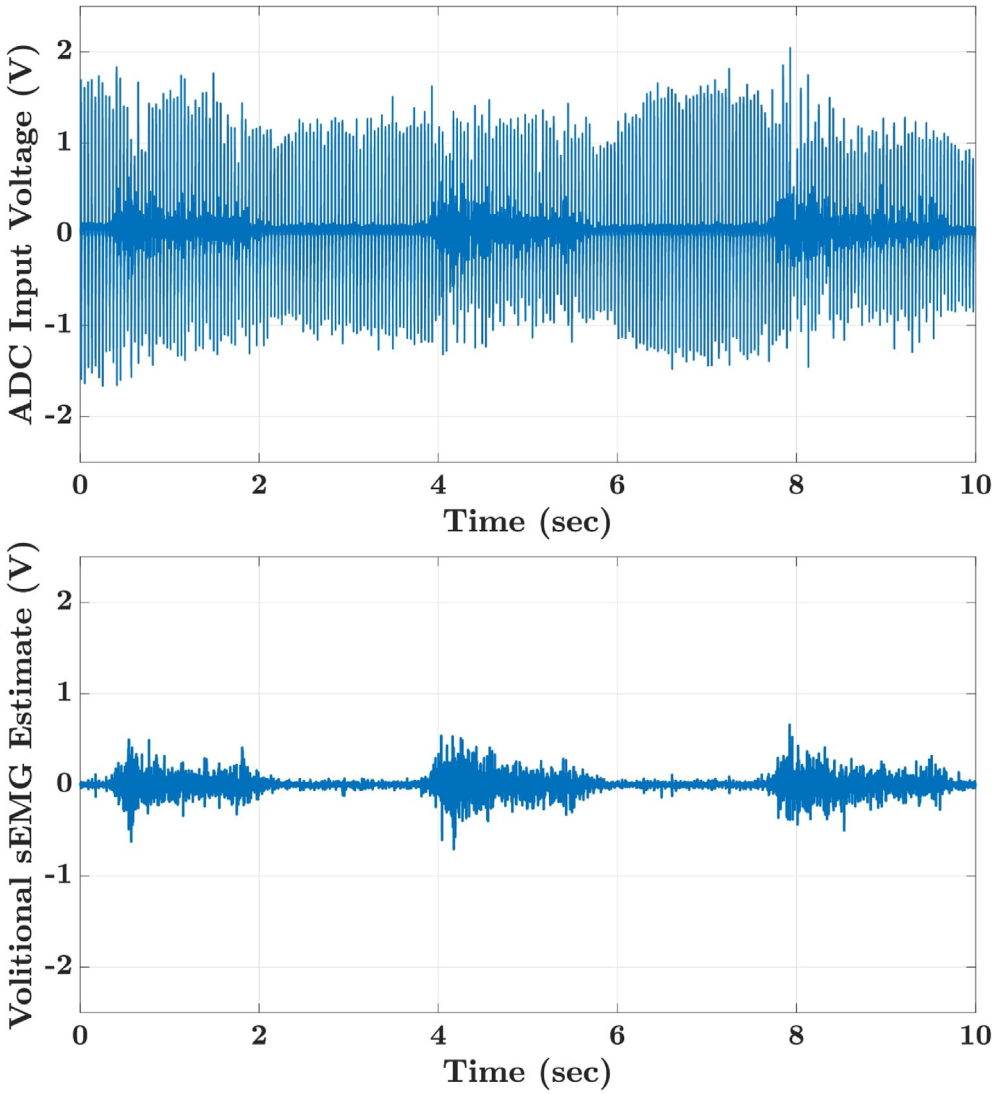

Fig. 9. Raw sEMG data recorded for one subject (top). Volitional sEMG estimate using adaptive algorithm [26] with six epochs.

periods (highlighted by the yellow shaded sections). These segments depict each subject's volitional sEMG data, superposed with the M-Wave artefact. The segments are manually selected to be at the start of volitional contraction. As such, there is a visible increase in the signal's baseline excitation between the first and third stimulation periods.

Conventional filtering techniques such as a comb or high-pass filter can be applied to isolate the M-Wave from volitional sEMG; however, these techniques have been shown to be less accurate than other techniques due to temporal and spectral overlap of the signals [27,28]. Implementation of an adaptive filter, such as that detailed by Sennels et al. [26], is recommended. The adaptive filter proposed by Sennels et al. [26] was applied to the raw sEMG data from Fig. 8 to provide an estimate of the subject's volitional sEMG. Fig. 9 (top) depicts the raw sEMG from one subject, superposed with their M-Wave. Fig. 9 (bottom) depicts the equivalent adaptive filter output, in which the subject's estimated M-wave artefact has been removed.

Human and animal rights

This study was approved by the Human Ethics Committee, University of Canterbury (HEC2020/68) and informed consent was obtained from each participant prior the experiment.

Declaration of Competing Interest

The authors declare that they have no known competing financial interests or personal relationships that could have appeared to influence the work reported in this paper.

Acknowledgements

This work was supported by Catalyst: Seeding funding, provided by the New Zealand Ministry of Business, Innovation and Employment and administered by the Royal Society Te Apārangi. Grant No. CSG-UOC190.

References

[1] R. Suhaimi, A.A.R, N.H. Adnan, D. Shahriman, J.A.A. Bakar, Analysis of EMG-based Muscles Activity for Stroke Rehabilitation, in: 2nd International Conference on ELectronic Design (ICED), 2014, pp. 167–170..
[2] J.V. Basmajian, C.J. De Luca, Muscles Alive: their Functions Revealed by Electromyography, Williams and Wilkins, 1979.
[3] L. Chatfield, B. Fortune, L. McKenzie, C. Pretty, Implementation of a particle filter to estimate torque from electromyography, in: IFAC, 2018, pp. 327–332..
[4] M. Cifrek, V. Medved, S. Tonković, S. Ostojić, Surface EMG based muscle fatigue evaluation in biomechanics, Clin. Biomech. 24 (4) (2009) 327–340.
[5] W. Rong, K.Y. Tong, X.L. Hu, S.K. Ho, Disability and Rehabilitation: Assistive Technology Effects of electromyography-driven robot-aided hand training with neuromuscular electrical stimulation on hand control performance after chronic stroke Effects of electromyography-driven robot-aided han, vol. 3107, no. April 2017, 2015..
[6] M.B.I. Reaz, M.S. Hussain, F. Mohd-Yasin, Techniques of EMG signal analysis: detection, processing, classification and applications (Correction), Biol. Procedures Online 8 (1) (2006), pp. 163–163.
[7] R. Luo, Can the voluntary drive to a paretic muscle be estimated from the myoelectric signal during stimulation? PhD thesis, 2013..
[8] B. Fortune, C. Pretty, L. Chatfield, L. McKenzie, M. Hayes, Low-cost active electromyography _ Elsevier Enhanced Reader.pdf, HardwareX, vol. 6, no. 1, 2019..
[9] R. Futami, K. Seki, T. Kawanishi, T. Sugiyama, I. Cikajlo, Y. Handa, Application of local EMG-driven FES to incompletely paralyzed lower extremities, 10th Annual Conference of the International FES Society July 2005 – Montreal, Canada, no. July, pp. 3–5, 2005..
[10] R. Shalaby, T. Shauer, L. Wolfgang, J. Raisch, Amplifier design for EMG recording from stimulation electrodes during functional electrical stimulation leg cycling ergometry, Biomed. Technol. 56 (1) (2011) 23–33.
[11] E. Ambrosini, S. Ferrante, M. Tibiletti, T. Schauer, C. Klauer, A. Pedrocchi, Support: a preliminary study, 2011, pp. 4259–4262..
[12] X. Yi, J. Jia, S. Deng, S.G. Shen, Q. Xie, G. Wang, A blink restoration system with contralateral EMG triggered stimulation and real-time artifact blanking, IEEE Trans. Biomed. Circuits Syst. 7 (2) (2013) 140–148.
[13] P. Taylor, P. Chappell, An investigation of the inhibition of voluntary EMG activity by electrical stimulation of the same muscle, FESnet, vol. 44, no. 0, 2003..
[14] H. Yeom, Y.-H. Chang, Autogenic EMG-controlled functional electrical stimulation for ankle dorsiflexion control, 193(1) (2011) 118–125..
[15] J. Nishida, K. Suzuki, bioSync, in: Proceedings of the 2017 CHI Conference on Human Factors in Computing Systems – CHI '17, 2017, pp. 3316–3327..
[16] S.F. del Toro, Y. Wei, E. Olmeda, L. Ren, W. Guowu, V. Díaz, Validation of a low-cost electromyography (EMG) system via a commercial and accurate EMG device: pilot study, Sensors (Switzerland) 19 (23) (2019) 1–16.
[17] T. Ye, Precision Full-Wave Rectifier, Dual-Supply, Tech. Rep. 1, Texas Instruments, Dallas, 2013..
[18] N.C. Chester, W.K. Durfee, Surface EMG as a fatigue indicator during FES-induced isometric muscle contractions, J. Electromyogr. Kinesiol. 7 (1) (1997) 27–37.
[19] J. Minzly, J. Mizrahi, N. Hakim, A. Liberson, Stimulus artefact suppressor for EMG recording during FES by a constant-current stimulator, Med. Biol. Eng. Comput. 31 (1) (1993) 72–75.
[20] K.C. Megill, K.L. Cummins, L.J. Dorfman, B.B. Berlizot, K. Luetkemeyer, D.G. Nishimura, B. Widrow, On the nature and elimination of stimulus artifact in nerve signals evoked and recorded using surface electrodes, IEEE Trans. Biomed. Eng. BME-29(2) (1982) 129–137..
[21] E.a. Brown, J.D. Ross, R.a. Blum, Y. Nam, B.C. Wheeler, S.P. Deweerth, Stimulus artifact elimination in a multi-electrode system, IEEE Trans. Biomed. Circuits Syst. 2(1) (2008) 10–21..
[22] F. Widjaja, C.Y. Shee, P. Poignet, W.T. Ang, FES artifact suppression for real-time tremor compensation, in: 2009 IEEE International Conference on Rehabilitation Robotics, ICORR 2009, 2009, pp. 53–58..
[23] C. Frigo, M. Ferrarin, W. Frasson, E. Pavan, R. Thorsen, EMG signals detection and processing for on-line control of functional electrical stimulation, J. Electromyogr. Kinesiol. 10 (5) (2000) 351–360.
[24] D. Zhang, W.T. Ang, Reciprocal EMG controlled FES for pathological tremor suppression of forearm, in: Annual International Conference of the IEEE Engineering in Medicine and Biology – Proceedings, no. 1, 2007, pp. 4810–4813..
[25] T. Schauer, T. Seel, N.D. Bunt, P. Müller, J.C. Moreno, Realtime EMG analysis for transcutaneous electrical stimulation assisted gait training in stroke patients, IFAC-PapersOnLine 49 (32) (2016) 183–187.
[26] S. Sennels, F. Biering-Sorensen, S. Hansen, O. Andersen, Adaptive filters for muscle response suppression, in: Proceedings of 18th Annual International Conference of the IEEE Engineering in Medicine and Biology Society, vol. 2, 1996, pp. 518–520..
[27] T. Al-ani, F. Cazettes, S. Palfi, J.P. Lefaucheur, Automatic removal of high-amplitude stimulus artefact from neuronal signal recorded in the subthalamic nucleus, J. Neurosci. Methods 198 (1) (2011) 135–146.
[28] L.F. Heffer, J.B. Fallon, A novel stimulus artifact removal technique for high-rate electrical stimulation, J. Neurosci. Methods 170 (2) (2008) 277–284.